WRAP: An open-source kinematic aircraft performance model

Junzi Sun[a,*], Joost Ellerbroek[a], Jacco M. Hoekstra[a]

[a]*Faculty of Aerospace Engineering, Delft University of Technology,*
Kluyverweg 1, 2629 HS, Delft, the Netherlands

Abstract

Open access to flight data from Automatic Dependent Surveillance-Broadcast (ADS-B) has provided researchers with more insights for air traffic management than aircraft tracking alone. With large quantities of trajectory data collected from a wide range of different aircraft types, it is possible to extract accurate aircraft performance parameters. In this paper, a set of more than thirty parameters from seven distinct flight phases are extracted for common commercial aircraft types. It uses various data mining methods, as well as a maximum likelihood estimation approach to generate parametric models for these performance parameters. All parametric models combined can be used to describe a complete flight that includes takeoff, initial climb, climb, cruise, descent, final approach, and landing. Both analytical results and summaries are shown. When available, optimal parameters from these models are also compared with the Base of Aircraft Data and the Eurocontrol aircraft performance database. This research presents a comprehensive set of methods for extracting different aircraft performance parameters. It also provides the first set of open parametric performance data for common aircraft types. All model data are published as open data under a flexible open-source license.

Keywords: aircraft performance, kinematic model, ADS-B, data mining, data analytics

*Corresponding author
Email address: j.sun-1@tudleft.nl (Junzi Sun)

Nomenclature

a_*	Acceleration or deceleration (m/s^2)
d_*	Distance (takeoff or landing) (km)
D	D score of Kolmogorov-Smirnov test (-)
h_*	Aircraft altitude (km)
M_*	Mach number (-)
R_*	Flight range (km)
$V_{eas,*}$	Equivalent air speed (m/s)
$V_{cas,*}$	Calibrated air speed (m/s)
$V_{tas,*}$	True air speed (m/s)
VS_*	Vertical speed (m/s)

TO/to	Aircraft takeoff phase
IC/ic	Aircraft initial climb phase
CL/cl	Aircraft climb phase
CR/cr	Aircraft cruise phase
DE/de	Aircraft descent phase
FA/fa	Aircraft final approach phase
LD/ld	Aircraft landing phase

ADS-B	Automatic Dependent Surveillance-Broadcast
APM	Aircraft performance model
ATM	Air traffic management
BADA	Base of aircraft data
CAS	Calibrated airspeed
CDA	Continuous descent approach
ISA	International standard atmosphere
PDF	Probability density function
ICAO	International Civil Aviation Organization

1. Introduction

Fast-time air traffic simulation requires accurate aircraft performance models (APM). These performance models play an important role in modeling and optimizing air traffic flows, especially in managing 4D trajectories. Traditionally, aircraft performance models for air traffic management (ATM) research are built based on manufacturer performance reports and/or proprietary flight data. As these data sources are either costly or have certain license limitations. The most commonly used APM, Base of Aircraft Data (BADA) family 3, has license limitations (Nuic, 2009), while the newer version of BADA family 4 (Gallo et al., 2006) comes with even stricter license agreements. Besides BADA, aircraft manufacturers also provide performance models. Unfortunately, though, very few of these are available as open-access models. These restrictions in obtaining and using aircraft performance models make it difficult to implement comparison studies and undertake research validations within the ATM community.

A different approach to model aircraft performance is to use flight data. An recent study of Hrastovec and Solina (2016) proposes to obtain performance parameters and patterns using radar data and machine learning methods. At the same time, thanks to the mandates on aircraft Auto-

matic Dependent Surveillance-Broadcast (ADS-B) transponders from different regulatory agencies around the world, an increasing number of commercial aircraft are being equipped with this capability. Low-cost ground receivers are being installed around the world in a crowd-sourced fashion. As a result, open flight data has become more accessible. With ADS-B, certain surveillance data such as position, altitude, velocity, and vertical speed are broadcast and received constantly around the world by a number of ground receiver networks.

Several leading crowd-sourced ground networks are providing free access to aggregated ADS-B data. Commercial networks like FlightRadar24 and FlightAware have large infrastructure and coverage. Research networks such as ADS-B Exchange and the OpenSky Network (Schäfer et al., 2014) are also expanding. Each network has a different policy on data sharing. However, many of these networks grant the rights of data usage to network contributors. These large amounts of raw flight data provide a new source for modeling aircraft performance.

How we can use these large quantities of data in order to construct aircraft performance models is the core research question of this paper. This paper aims to construct an accurate kinematic performance model for common aircraft types and then employ such a model for air traffic simulation and analysis.

There are different categories of performance models. The most detailed six degree-of-freedom model is commonly used in aircraft control studies, while the point-mass model is often used in studies concerning air transportation. In the point-mass model, aircraft roll, pitch, and yaw motions are ignored, leaving only horizontal and vertical motions. There are two different types of point-mass models: kinetic and kinematic. The primary difference is that while a kinetic model focuses on forces and energy, a kinematic model deals only with aircraft motions. BADA, for instance, employs both model types: the BADA aircraft performance operation file (OPF) models the kinetic properties of the aircraft, while the airline procedures file (APF) models the kinematic aspects of flights. Also developed by the Eurocontrol, the General Aircraft Modelling Environment (GAME) is another kinematic performance model (Calders, 2002). Both kinetic and kinematic models have their advantages and disadvantages. For example, the kinematic approach is simpler by removing the forces in the performance model. But it is not suitable in, for example, studies of aircraft trajectory prediction or optimization of individual flight. Though we are also aiming to construct open kinetic models in other studies, the models proposed in this paper are purely kinematic point-mass models.

In real flights, no two trajectories are identical. With every aircraft type, different degrees of performance deviation are always present. The performance often differ even within the same flight phase for different flights. The main causes for this variation include variability in aircraft mass, thrust settings, wind, and flight procedures. Transmission error and data source uncertainty can also contribute to these deviations. The biggest challenge that is addressed in this paper is how to extract useful information from a large quantity of flight data. As an aircraft can perform differently in each flight phase, flight data need to be segmented accordingly. Machine learning and data mining methods, as proposed by our earlier research, provide efficient ways to process the time series data into organized segments, based upon trajectory and respective flight phases (Sun et al., 2017a). In this paper, the generated output data is further divided into detailed segments according to the model definitions proposed in this paper.

Based on our preliminary research (Sun et al., 2017b), this paper proposes a kinematic aircraft performance model based entirely on open data, called the WRAP performance model. In addition to common procedural values, a parametric statistical model of each performance indicator is constructed. The use of parametric statistical models enables probabilistic sampling in simulations and produces realistic scenarios. Thanks to this unique property, the model can cover a wide range

of use cases.

The remainder of this paper is structured as follows. Section two introduces the model parameters, definitions, and maximum likelihood estimations for three different distribution functions. Section three explains the data and pre-processing methods. Section four is focused on methods and algorithms for constructing parameters of each flight phase. Detailed results on a single aircraft type and summaries of 17 different aircraft types are shown in section five. Finally, discussions and conclusions are addressed in sections six and seven.

2. The WRAP model

In this section, the kinematic aircraft performance parameters of the WRAP model are first presented. Based on flight data, each parameter is evaluated under three parametric statistical model assumptions. We then choose the best statistical model according to the Kolmogorov-Smirnov test (Massey Jr, 1951), from which the optimal and limitation values are computed.

2.1. Model parameters

Similar to the flight phase definitions from the International Civil Aviation Organization (ICAO) Common Taxonomy Team (Commercial Aviation Safety Team / Common Taxonomy Team, 2013), this research aims to derive performance parameters for the following flight phases: takeoff, initial climb, climb, cruise, descent, final approach, and landing. In the WRAP model, the definitions of the initial climb and final approach are slightly different from the ICAO definitions. This is because the WRAP model tries to generalize the parameters over different air traffic control procedures. These new definitions would limit the amount of influence due to human factors in the respective flight phases.

The significance of each performance indicator differs from one flight phase to another. For example, vertical speed is only of interest for climb and descent, while during takeoff and landing, the runway distance, acceleration, and takeoff/touchdown speed are studied. Specifically, during the climb (or descent) phase, a constant calibrated airspeed (CAS) and Mach number profile is extracted. The parameters included in the WRAP model are listed as follows per fight phase:

- Takeoff:
  - liftoff speed (V_{lof})
  - takeoff distance (d_{tof})
  - mean takeoff acceleration ($\bar{a}_{tof}$)
- Initial climb:
  - calibrated airspeed ($V_{cas,ic}$)
  - vertical rate (VS_{ic})
  - cutoff altitude (h_{ic}), fixed at 457m / 1500ft
- Climb:
  - range to the top of climb ($R_{top,cl}$)
  - constant CAS crossover altitude ($h_{cas,cl}$)
  - constant CAS ($V_{cas,cl}$)
  - vertical rate during constant CAS climb ($VS_{cas,cl}$)
  - constant Mach climb crossover altitude ($h_{mach,cl}$)
  - constant Mach number (M_{cl})
  - vertical rate during constant Mach climb ($VS_{mach,cl}$)
  - vertical rate before constant CAS climb ($VS_{precas,cl}$)

- Cruise:
  - cruise range (R_{cr})
  - maximum cruise range ($R_{max,cr}$)
  - initial cruise altitude ($h_{init,cr}$)
  - cruise altitude (h_{cr})
  - maximum cruise altitude ($h_{max,cr}$)
  - cruise Mach number (M_{cr})
  - maximum cruise Mach number ($M_{max,cr}$)
- Descent:
  - range from the top of descent ($R_{top,de}$)
  - constant Mach number (M_{de})
  - constant Mach descent crossover altitude ($h_{mach,de}$)
  - vertical rate during constant Mach descent ($VS_{mach,de}$)
  - constant CAS ($V_{cas,de}$)
  - constant CAS crossover altitude ($h_{cas,de}$)
  - vertical rate during constant CAS descent ($VS_{cas,de}$)
  - vertical rate after constant CAS descent ($VS_{postcas,de}$)
- Final approach:
  - calibrated airspeed ($V_{cas,fa}$)
  - vertical rate (VS_{fa})
  - cutoff altitude (h_{fa}), fixed at 300m / 1000ft
  - path angle ($\angle_{fa}$)
- Landing:
  - touchdown speed (V_{tcd})
  - braking distance (d_{lnd})
  - mean braking deceleration ($\bar{a}_{lnd}$)

One of the reasons behind the selection of these parameters is to ensure compatibility and comparability with existing kinematic performance models, such as the, the Aircraft Performance Database (EuroControl, 2017), as well as the kinematic parameters of BADA (Nuic, 2009). The WRAP model parameters were also designed with the aim of supporting the open air traffic simulator BlueSky (Hoekstra and Ellerbroek, 2016). The parameters are chosen so that the kinematic flight envelope of different aircraft models can be constructed according to the flight phases.

2.2. Parametric statistical models and selection

Three continuous probability density functions (PDF) are proposed to describe each of the performance parameters: the Normal, Gamma, and Beta distributions. Many of the performance parameters, for example, mean speed or mean vertical rates, can be modeled using a Normal distribution. Empirical observations with flight data support this claim, as does the central limit theorem in the probability theory. The theorem states that when independent random variables are drawn independently, the distribution of the averages trends to follow Normal distributions. In cases where human decisions are involved, however, the normal distribution may not be the best choice to describe a parameter. For example, with cruise range, or crossover altitude of constant CAS/Mach climb, the distribution can be skewed. Therefore, we need to introduce skewed distributions to model these parameters. The Gamma distribution and Beta distribution are used for right-skewed and left-skewed distributions respectively. Finally, the maximum likelihood estimation (MLE) (Aldrich et al., 1997) is used to estimate the best-unbiased model parameters under each statistical model assumption.

2.2.1. Normal distribution

For a Normal distribution, the PDF is expressed as:

$$p(x|\mu,\sigma^2) = \frac{1}{\sqrt{2\sigma^2\pi}} e^{-\frac{(x-\mu)^2}{2\sigma^2}} \tag{1}$$

where the parameters μ and, σ^2 represent the mean and variance. The MLE estimator of $\hat{\mu}$ and $\hat{\sigma}^2$ can be computed as the mean and variance of the observations.

2.2.2. Gamma distribution

For a standardized Gamma distribution with support of $(0, +\infty)$, the PDF is expressed as:

$$p(x|\alpha) = \frac{1}{\Gamma(\alpha)} x^{\alpha-1} e^{-x} \tag{2}$$

where α ($\alpha > 0$) represents the shape of the distribution. As a general form, the location (μ) and scale (k) parameters are introduced to allow the support of $(\mu, +\infty)$ for the PDF:

$$p(x|\alpha,\mu,k) = \frac{1}{k\cdot\Gamma(\alpha)} \left(\frac{x-\mu}{k}\right)^{\alpha-1} \exp\left(-\frac{x-\mu}{k}\right) \tag{3}$$

The MLE estimate $(\hat{\alpha}, \hat{\mu}, \hat{k})$ does not have a closed-form solution, but it can be solved numerically (Choi and Wette, 1969).

2.2.3. Beta distribution

For a standardized Beta distribution with support $(0, 1)$, the PDF is given as:

$$\begin{aligned} p(x|\alpha,\beta) &= \frac{1}{B(\alpha,\beta)} x^{\alpha-1}(1-x)^{\beta-1} \\ B(\alpha,\beta) &= \frac{\Gamma(\alpha)\Gamma(\beta)}{\Gamma(\alpha+\beta)} \end{aligned} \tag{4}$$

where α and β represent the shape of the distribution. As a general form, the location (μ) and scale (k) parameters can also be introduced to allow the support of $(\mu, +\infty)$ for the PDF:

$$p(x|\alpha,\beta,\mu,k) = \frac{1}{k\cdot B(\alpha,\beta)} \left(\frac{x-\mu}{k}\right)^{\alpha-1} \left(1-\frac{x-\mu}{k}\right)^{\beta-1} \tag{5}$$

Similar to the Gamma distribution, it also does not have a closed-form solution for the MLE estimate $(\hat{\alpha}, \hat{\beta}, \hat{\mu}, \hat{k})$, and, therefore, also needs to be solved numerically (Gnanadesikan et al., 1967).

2.2.4. Selection of the statistical model

After all possible optimal parametric models are computed based on test data, the best of all three are identified using the D score from the one-sample Kolmogorov-Smirnov (KS) Test (Massey Jr, 1951).

$$D = \max_x |F_n(x) - F(x)| \tag{6}$$

where $F(x)$ is the cumulative distribution function (CDF) of a statistical model and $F_n(x)$ is the the empirical distribution function (EDF) from the data. The D score is essentially the largest distance between two functions, which is calculated according to Equation 6. A smaller D score reveals a better fit of the statistical model toward the test data.

Of all three KS statistics $D_{\mathcal{N}}$, D_{Γ}, and D_B, the probability density that yields the minimum D will be selected. The KS-test is performed on a different dataset that was used for the parameter estimation. In this paper, the experiment data is split into two equal parts (one for fitting and one for testing) to construct and validate the best parametric statistical model.

An example data set of one parameter is shown in Fig. 1, where the CDF of all three models obtained from MLE is displayed against the EDF computed from the data. The best model (beta) is obtained, as it yields the lowest D score in this example.

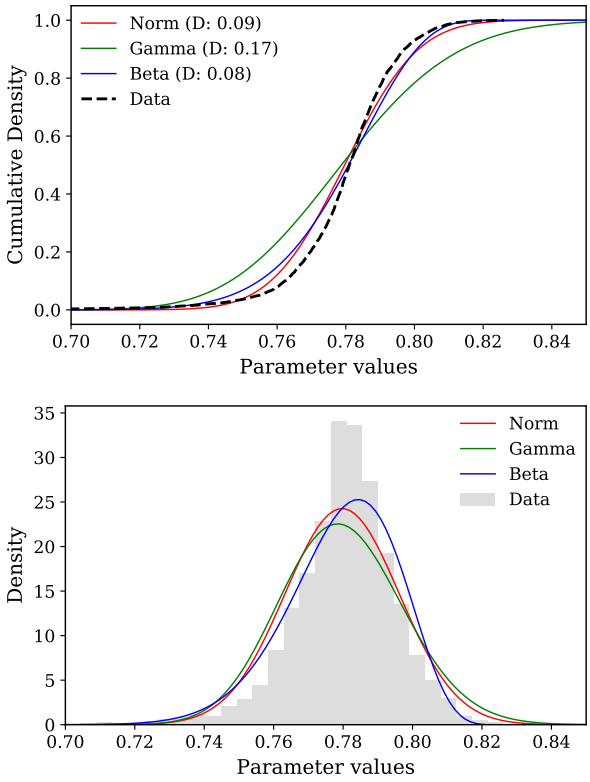

Figure 1: Cumulative distributions and probability distributed of fitted model with data. The example parameter is the mean cruise Mach number of A320 aircraft type. The best model describing the data is Beta distribution that yields the minimum D value of 0.08.

2.3. Interpretation of the model

In the resulting WRAP model, each parameter is described with three parts using the following convention:

$$\left\{\hat{\psi} \mid \psi_{min}, \psi_{max} \mid \text{*pdf}\right\} \tag{7}$$

The first part, $\hat{\psi}$ is the optimal value. The optimal value is computed as the mode of the probability distribution function, which corresponds to the most frequent value in reality. It is important to emphasize that the optimal value obtained from the distribution is not necessarily the optimal performance value for an individual flight.

The second part, ψ_{min} and ψ_{max}, are minimum and maximum values obtained from different confidence intervals (CI). The CI is defined based on the parameter type:

- CI=0.85: Parameters associated with speed during takeoff, initial climb, final approach, and landing.

- CI=0.99: Parameters associated with ranges.
- CI=0.9: Default value of other parameters.

Here, the choice of a low confidence interval for velocity parameters is made to reduce the impact of wind uncertainties in flight phases that are close to the ground. Even though the wind data has already been integrated, wind information is less certain for near-surface conditions. Thus the low CI is chosen. The choice of a higher CI for flight ranges is made to take into account flights with a range as close to their maximum operational range as possible. The hypothesis is that extreme values are likely not outliers when dealing with flight range.

The third part in Equation 7 is the optimal statistical model that is obtained from the KS test. It is defined as:

$$*\text{pdf} = \begin{cases} ['norm', \mu, \sigma] & \text{for } x \sim \mathcal{N} \\ ['gamma', \alpha, \mu, k] & \text{for } x \sim \Gamma \\ ['beta', \alpha, \beta, \mu, k] & \text{for } x \sim B \end{cases} \tag{8}$$

Three types of values defined by the WRAP model provide different use cases. For example, in the case of conducting air traffic simulations (Hoekstra and Ellerbroek, 2016):

1. The optimal value can be used for air traffic simulations with a fixed performance profile. It can be considered as a standard airline procedure profile, which is equivalent to the APF in BADA model.
2. The minimum and maximum values define the limits of the kinematic model, which implements the flight envelopes.
3. The PDF provides the possibility of construct Monte-Carlo simulation or study where parameters need to be sampled according to a realistic probability distribution.

3. The data

When dealing with aggregated ADS-B flight data, errors often occur. Trajectory data need to be pre-processed and segmented by flight phase accordingly. At the same time, not all parameters can be directly observed. To infer those hidden parameters, certain models and methods need to be designed. In the following two sections, we discuss the methods used for data processing and performance modeling.

3.1. Data source

For this research, the input data are primarily based on ADS-B messages that are broadcast by aircraft through Mode-S transponders. However, even with good installation and placement, a single ground-based receiver only has a maximum reception range of around $250nm$ ($\sim 500km$). Considering Mode-S line-of-sight availability, it is not possible to capture large quantities of completed flight data with a single ground station. This is especially challenging when dealing with long-range flights. Thanks to networks of ADS-B ground receivers, such as FlightRadar24 (FlightRadar24 AB, 2017), it is possible to gain access to a much larger collection of flight data obtained from ground stations from contributors around the world.

It is also worth noting that in addition to ADS-B data, using the same receiver setup, aircraft positions and velocities can be also obtained from multiple ground stations using Mode-S multilateration. This technology is employed by some ground receivers within the FlightRadar24 network.

It is useful for those aircraft that are not yet equipped with ADS-B compatible transponders. However, the availability is limited to areas where air traffic controllers are present and not usable when aircraft are close to the ground.

3.2. Trajectory processing

Data collected from ADS-B are usually scattered. Previous machine learning methods proposed by Sun et al. (2017a) have made it possible to extract flight trajectories easily. However, this method can only segment flights into four different phases: on-ground, climb, cruise, and descent.

The work in this paper requires further processing of those segments. To this end, an altitude threshold is applied to the climb and descent trajectory to extract the initial climb and final approach. We consider the climbing section up to 1500 ft to be the initial climb. The final approach starts from 1000 ft toward the end of the descent. Secondly, to avoid the level-flight segments in climb or descent phases being identified as the cruise, we consider that the cruise segment lasts less than five minutes to be level-flight segments. This threshold is selected empirically based on our analysis of a large number of flights. Lastly, an evaluation process is used to examine the data of all flight segments, ensuring a certain level of completeness and continuity in the given time series data.

To ensure the trajectories selected are matched with correctly identify phases, we employ the validation method proposed in Sun et al. (2017a), which checks the number of altering phases. We then examine the altitude at the start and end of each flight phase, as well as the number of data points presented in each phase.

3.3. Atmospheric conditions and speed conversions

The velocity provided in an ADS-B message gives the ground speed of an aircraft. However, the accuracy of the model may be compromised as wind is not considered. For example, the seasonal wind and jet streams cause a great bias when modeling the cruise speed, if only the ground speed is considered. In this paper, wind speeds are computed using an interpolation model from Global Forecast System (GFS) Reanalysis data (Saha et al., 2010).

The GFS Analysis model cycles every six hours, producing atmospheric grids using global data assimilation. The grid data are stored at two resolutions (0.5 and 1 degree). Vertically, isobaric levels from 1000hPa to 10hPa are provided, divided into 26 layers. In this paper, the U component (west-east direction) and V component (south-north direction) of wind, as well as the temperature of all grid points, are extracted from the datasets. Then 4-D (latitude, longitude, altitude, and time) grids for wind and temperature are constructed. Figure 2 shows an example of the wind grid snapshot.

After that, an N-dimensional multi-linear interpolation (Weiser and Zarantonello, 1988) is used to construct a linear 4-D interpolated model. As such, wind and temperature can be produced at any position and time. ADS-B positions of all aircraft are mapped with wind vectors from the model to produce the corresponding airspeeds. Figure 3 illustrates an example of the airspeed versus ground speed of aircraft, where the difference is obvious in some locations.

The WRAP model uses Mach number (M) and calibrated airspeed (V_{cas}) when appropriate. Mach number can be computed using the following equation:

$$M = \frac{V_{tas}}{a} = \frac{V_{tas}}{a_0\sqrt{\frac{T}{T_0}}} \tag{9}$$

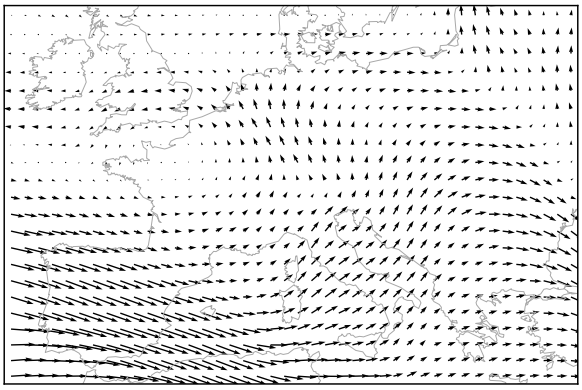

Figure 2: Example of wind over Europe at 400hPa pressure level of GFS model (23.5 kft, ISA+0°C)

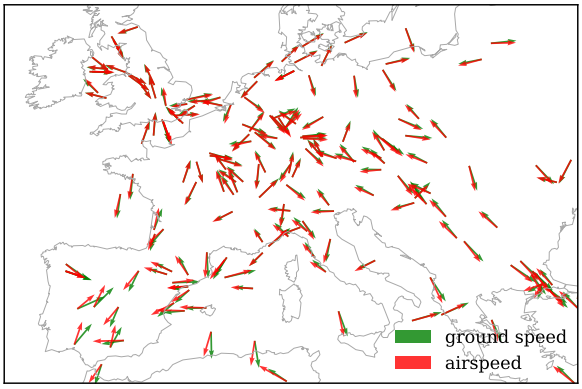

Figure 3: Example aircraft ground speed and airspeed difference (cruising aircraft above 20k ft)

where T_0 and a_0 are temperature and speed of sound at ISA sea level. T and a are the air temperature and speed of sound at the location of the aircraft. The air pressure can be derived from the barometric altitude obtained using ADS-B:

$$p = p_b \left[1 + \frac{\lambda(h - h_b)}{T_b}\right]^{\frac{-g}{\lambda R}} \qquad \lambda \neq 0 \tag{10}$$

$$p = p_b \exp\left[-\frac{g(h - h_b)}{RT_b}\right] \qquad \lambda = 0 \tag{11}$$

where h is the pressure altitude of the aircraft. λ is lapse rate (-6.5 K/km for troposphere). h_b is the base altitude, which is 0 km or 11 km for troposphere or tropopause respectively. p_b is the base pressure, which is 101,325 Pa or 22,632 Pa for troposphere or tropopause respectively. T_b is the base temperature, which is 288.15 K or 216.65 K for troposphere or tropopause respectively. Knowing the pressure and Mach number, we can compute the calibrated airspeed as follows (Young, 2017, section 6.6.4):

$$V_{cas} = a_0 \sqrt{5\left\{\left[\frac{p}{p_0}\left\{(1 + 0.2M^2)^{3.5} - 1\right\} + 1\right]^{\frac{1}{3.5}} - 1\right\}} \tag{12}$$

4. Construction of WRAP parameters

After the flight trajectories are sorted and segmented in proper flight phases, they can be used to construct the desired model parameters. For each aircraft type, at least five thousand trajectories are used to give a good level of confidence in the model. This section discusses the methods for extracting these parameters from the trajectory data.

4.1. Takeoff

During the takeoff phase, the parameters of most interest are takeoff distance (D_{tof}), mean acceleration ($\bar{a}_{tof}$), and lift-off speed (V_{lof}). To overcome the large noise in the velocity measurements during takeoff, a second-degree spline is applied to obtain a smoothed velocity sample set. The distance parameters can be derived from aircraft surface position at the starting and ending positions of the takeoff, using the spherical law of cosines, based on the dot product of the vectors from the center of the earth to the positions:

$$D_{tof} = R \cdot \arccos[\sin\phi_1 \cdot \sin\phi_N + \cos\phi_1 \cdot \cos\phi_N \cdot \cos(\lambda_N - \lambda_1)] \tag{13}$$

where ϕ and λ represent the latitude and longitude in radians. 1 and N represent the first and last recorded position during takeoff. The average acceleration $\bar{a}_{tof}$ is obtained from a second-order polynomial fitting, based on the time and speed measurements during the takeoff.

Compared to takeoff distance and average acceleration, the lift-off speed is more complicated to estimate, due to the low data update rate in an aggregated ADS-B dataset. There is usually a gap of a few seconds between the last on-ground data sample and the first in-air observation.

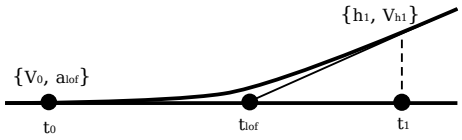

Figure 4: Estimate the lift off moment

To estimate the exact moment of lift-off, as shown in Fig. 4, an interpolation model is used. Firstly, the vertical rate VS and time stamp at the first in-air observation are used to estimate the time of lift-off t_{lof}. Combining this result with previously calculated $\bar{a}_{tof}$, the lift-off speed can be obtained as follows:

$$t_{lof} = t_1 - \frac{h_1}{VS_1} \tag{14}$$

$$V_{lof} = V_0 + \bar{a}_{tof} \cdot (t_{lof} - t_0) \tag{15}$$

4.2. Initial climb

The initial climb phase is defined as the segment from 35 ft until the aircraft reaches around 1500 ft. There are several major configuration changes (retraction of landing gear and flaps) during this short period of time that can affect the performance of the aircraft. However, because the initial climb segment lasts for only a short time, it suffers from having relatively few data samples, comparable to the takeoff phase. The parameters to be studied are aircraft calibrated airspeed ($V_{cas,ic}$) and vertical rate (VS_{ic}). Both parameters can be computed directly from ADS-B data.

4.3. Climb

The climb segment starts when the aircraft reaches clean configuration and lasts until the moment when it reaches cruise altitude. As a common practice, aircraft first accelerate to a target CAS and then fly according to this constant CAS. Mach number increases with the increasing true airspeed, as well as the effect of the decreasing speed of sound. When a certain Mach number is reached, an aircraft will fly according to this constant Mach number until its cruising altitude. During the Mach climb segment, a decreasing CAS will be observed due to the decreasing pressure and temperature.

The challenge is to identify the crossover between the constant CAS and constant Mach climb. Knowing the general profile of CAS and Mach number during the climb, it is possible to design a two-step and two-piecewise estimator for extracting this feature from CAS and Mach number profiles.

The crossover estimator consists of two parts: an increasing (quadratic or linear) segment and a constant segment. The quadratically increasing part is designed so that it resembles the general observation that velocity increases with a decreasing acceleration. The constant segment approximates constant CAS or Mach values. The estimator is expressed as follows:

$$f_{mach}(t) = \begin{cases} k_1 \cdot (t - t_{mach}) + y_{mach} & t \leq t_{mach} \\ y_{mach} & t \geq t_{mach} \end{cases} \tag{16}$$

$$f_{cas}(t) = \begin{cases} -k_2 \cdot (t - t_{cas})^2 + y_{cas} & t \leq t_{cas} \\ y_{cas} & t_{cas} \leq t \leq t_{mach} \end{cases} \tag{17}$$

To illustrate the modeling process, we use a two-step piecewise least-squares fitting as illustrated in Fig. 5.

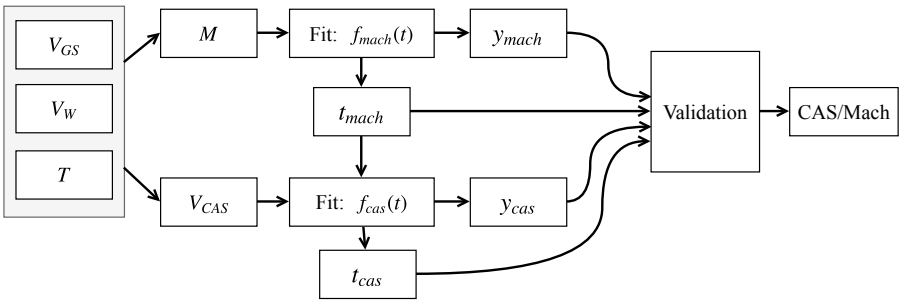

Figure 5: Constant CAS/Mach climb identification process

The entire climbing phase in terms of Mach number can be divided into two parts (increasing and constant). The first estimator applies on the entire climb data and uses a least-squares fitting to extract the best CAS/Mach crossover time t_{mach} and constant Mach climb number y_{mach}.

The second estimator uses t_{mach} as cutoff time, fitting the start of the time series until t_{mach}. This estimator is designed to obtain the constant CAS speed y_{cas} and its starting time t_{cas}. The crossover altitude is identified by extracting the actual altitude of the aircraft at time t_{mach}. We can also compute the theoretical crossover altitude ($\tilde{h}_{mach}$) from the y_{mach} and y_{cas} (Young, 2017,

section 17.2.2):

$$\begin{aligned} \tilde{h}_{mach} &= \frac{T_0}{L}\left(\delta^{\frac{-RL}{g_0}} - 1\right) \\ \delta &= \frac{\left[0.2\left(\frac{y_{cas}}{a_0}\right)^2 + 1\right]^{3.5} - 1}{\left(0.2y_{mach}^2 + 1\right)^{3.5} - 1} \end{aligned} \tag{18}$$

where T_0 and a_0 are temperature and speed of sound at sea level. R and L are specific gas constant and lapse rate. In this paper, we use this theoretical model to validate the obtained result. The complete validation model is defined as follows:

$$\begin{aligned} k_1 &> 0 \\ k_2 &> 0 \\ t_{cl,end} - t_{mach} &> 0.05\ (t_{cl,end} - t_{cl,start}) \\ t_{mach} - t_{cas} &> 0.05\ (t_{cl,end} - t_{cl,start}) \\ \mathrm{VAR}[V_{mach}] &< 0.02^2 \\ \mathrm{VAR}[V_{cas}] &< 10^2 \\ \frac{|h_{mach} - \tilde{h}_{mach}|}{\tilde{h}_{mach}} &< 0.05 \end{aligned} \tag{19}$$

where $t_{cl,start}$ and $t_{cl,end}$ are the timestamps of start and end of the climb, and VAR represents the variance of the parameter based all the data points in a constant segment. The first two questions ensure the correct model parameters k_1 and k_2 are identified. The second two equations ensure the constant segments last for more than 5% (an empirical value) of the climb duration. The last two conditions examine the variance the of all V_{cas} or V_{mach} during the constant segment. They ensure the variations of data values remain below certain thresholds.

To illustrate the entire process, this method is applied on one flight and shown in Fig. 6. The green and red colors represent the Mach and CAS profile during the climb, both with a constant segment that has been identified by the model.

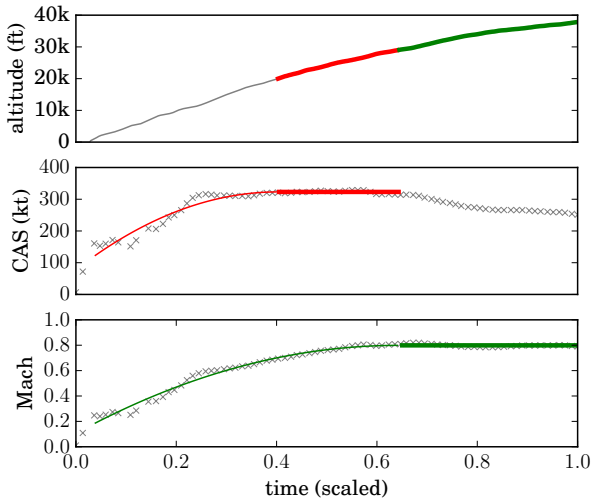

Figure 6: Constant CAS/Mach climb identification example

After t_{cas} and t_{mach} are determined, crossover altitudes $h_{cas,cl}$, $h_{mach,cl}$, at which the constant CAS and constant Mach climbing commence, can be obtained. Vertical rates $VS_{precas,cl}$, $VS_{cas,cl}$, $VS_{mach,cl}$ that correspond to these three segments can also be computed. In addition, range from takeoff to the top of climb $R_{top,cl}$ is calculated.

4.4. Cruise

Aircraft generally cruise at selected optimal flight levels that are often the most fuel efficient. Optimal cruise altitude changes as aircraft weight decreases and atmospheric condition alters. The calculation of the optimal cruise altitude requires the knowledge of thrust and drag forces, atmospheric conditions, as well as mass of the aircraft. Since the WRAP model deals with the kinematic parameters of the flight, we have to limit the scope of our model. The model focuses on describing the common and maximum values of altitude, speed, and range based on our data.

The common parameters to be modeled are the cruise altitude h_{cr} and cruise Mach number M_{cr}. These two parameters are computed as the mean values respectively during the flight. The initial cruise altitude $h_{init,cr}$ is also an interesting parameter that defines the top of the climb. It is computed as the average altitude during the first minute of the cruise.

Aircraft operational boundary conditions such as their maximum cruise altitude $h_{max,cr}$ and maximum cruise Mach number $M_{max,cr}$ are first computed as the maximum altitude and Mach number per flight. Then the maximum values of the flights from the same aircraft type are used to model the final boundary conditions in the WRAP model. It is worth noting that the obtained parameters representing operational boundary conditions are the maximum values occurring during the operation. They are often within the performance limitations provided by the aircraft manufacturer.

In addition, the cruise range R_{cr} is extracted as an operational reference parameter. Since aircraft rarely fly a direct route between the origin and destination airport, the flight range cannot be calculated as the great circle distance between origin and destination. Due to the noise inherited from onboard GPS receivers, position reports in ADS-B can contain errors (Mohleji and Wang, 2010). When integrating positions along the trajectory, the accumulated error may grow larger. Hence, a first order spline filter is implemented, and then the trajectory is re-sampled and integrated to produce the cruise range. This process is illustrated in Fig. 7, where the filtered trajectory is shown in red, as compared to real position reports in blue, and the great circle in the dashed black line.

4.5. Descent

The descent phase of the aircraft is comparable to the climb phase. From the top of descent, the aircraft undergoes a constant Mach and constant CAS descent segment before reaching the approach altitude.

The essential parameters to be modeled are: range from top of descent to destination $R_{tod,de}$, Mach number during constant Mach descent $v_{mach,de}$, CAS during constant CAS descent $v_{cas,de}$, crossover altitudes $h_{mach,de}$ and $h_{cas,de}$, and vertical rates $VS_{mach,de}$, $VS_{cas,de}$, and $VS_{postcas,de}$.

Similar to climb, the constant Mach/CAS descent performance can be modeled by piecewise estimators. It is possible to use the same process as described in Fig. 5. The Mach profile is described using two linear pieces. The CAS profile consists of a linear and quadratic piece due to the high non-linearity in speed for the final approach segment. The model can be described as follows:

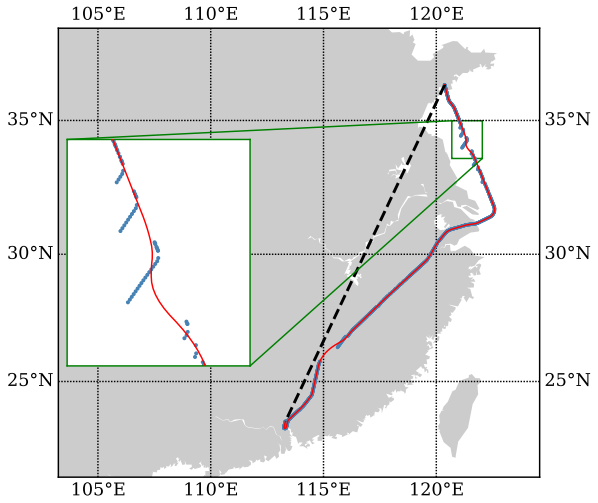

Figure 7: Cruise range spline filtering

$$f_{mach}(t) = \begin{cases} y_{mach} & t \leq t_{mach} \\ -k_1 \cdot (t - t_{mach}) + y_{mach} & t \geq t_{mach} \end{cases} \tag{20}$$

$$f_{cas}(t) = \begin{cases} y_{cas} & t_{mach} \leq t \leq t_{cas} \\ -k_2 \cdot (t - t_{cas})^2 + y_{cas} & t \geq t_{cas} \end{cases} \tag{21}$$

Similarly, the result of such a model as applied on one flight is shown in Fig. 8.

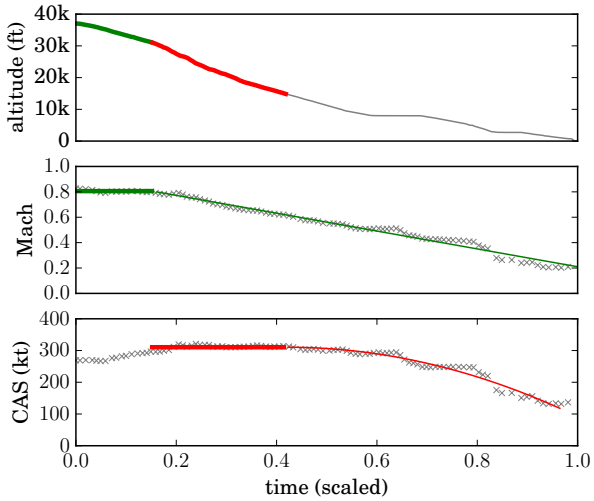

Figure 8: Constant CAS/Mach descent identification example

At lower traffic densities, it can occur that aircraft follow a so-called Continuous Descent Approach (CDA), which eliminates level-flight segments to reduce fuel consumption and engine noise. Such an approach affects the result of the aircraft performance in descent. This effect is discussed in section 7.5 in this paper.

4.6. Final Approach

Due to different control procedures at each airport, it is not easy to generalize the entire approach segment solely based on flight data. However, the final approach segment from around 1,000 ft until landing can be modeled.

The segment of the final approach represents the end of a descent, where aircraft operate at a nearly constant airspeed and rate of descent. The approach speed $V_{cas,fa}$ and Rate of descent $V_{h,fa}$ are modeled. In addition, the final approach path angle $\angle_{fa}$ is calculated.

4.7. Landing

The landing model is comparable with the takeoff model. Parameters such as touchdown speed V_{tcd}, braking distance d_{lnd}, average braking deceleration a_{lnd} of the aircraft are modeled similarly to the takeoff phase. Approach speed V_{tcd} can be observed from the last in-air velocity. Braking distance can be calculated using Equation 13, and average deceleration can be calculated similarly to takeoff acceleration.

5. Results

For this paper, the proposed methods have been applied to 17 common aircraft types. Sufficient data were collected for all aircraft. For each aircraft type, this represents around 5000 sets of data per flight phase. In order to better illustrate the modeling of each individual parameter, detailed results from a single aircraft type (Airbus A320) are described according to the previous model specification. A summary of the results for other aircraft types is shown in Table 2.

5.1. An Airbus A320 example

For each parameter, all three probability density functions (Normal, Gamma, and Beta) are applied using MLE. The best model is chosen and represented by different colors in all figures, shown in red, green, and blue respectively. $\hat{\psi}$, ψ_{min}, and ψ_{max} are also marked in each of the plots accordingly.

5.1.1. Takeoff

Three performance parameters D_{tof}, V_{lof}, and $\bar{a}_{tof}$ are shown in Fig. 9, where the most common values of these parameters are 1.65 km, 165 kt, and 1.93 $\mathrm{m/s^2}$, respectively.

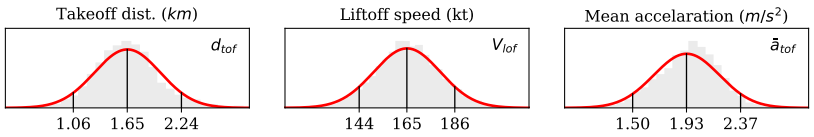

Figure 9: Takeoff parameters

5.1.2. Initial climb

Two performance parameters $V_{cas,ic}$ and VS_{ic} of the initial climb, up to the altitude of 1500ft, are shown in the first two plots of Fig. 10, where the most common values are 161 kt and 2477 ft/min.

The evidence for quasi-constant airspeed and vertical rate assumption can be seen from the standard deviations per trajectory, shown in the last two plots. It should also be noted that, in general, the vertical rate has larger variances. This is due to the fact that data sources for vertical rate commonly contain a certain degree of uncertainty (Hempe, 2010).

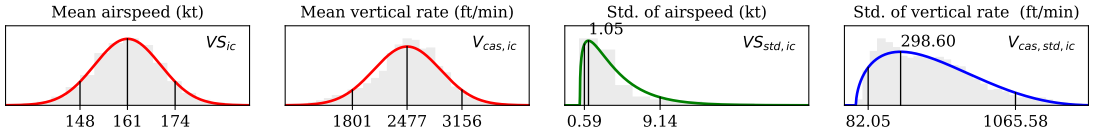

Figure 10: Initial climb parameters

5.1.3. Climb

Within the climb phase, the objective is to model the constant CAS/Mach climb profile, as well as the vertical rates in each of the segments of the profile. All parameters are shown in Fig. 11. Most commonly, before the aircraft accelerates to a constant calibrated airspeed of 293 kt, it has a mean climbing rate of 2016 ft/min. Once reaching the altitude of approximately 12 kft, the aircraft then climbs at 1600 ft/min until reaching a constant Mach number of 0.78 at the crossover altitude of 28.9 kft. After that, the aircraft climbs at 1039 ft/min until reaching the cruise altitude. The flight range of the climb phase is also shown in the last plot, which is typically around 257 km.

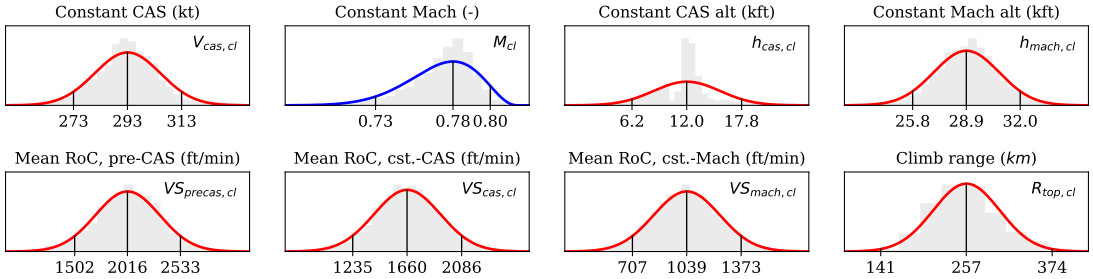

Figure 11: Climb parameters

5.1.4. Cruise

During the cruise phase, cruise Mach number M_{cr}, altitude h_{cr}, and cruise range R_{cr} are shown in Fig. 12 respectively. Maximum cruise Mach number $M_{max,cr}$ and maximum cruise altitude $h_{max,cr}$ can be obtained as the maximum value of M_{cr} and h_{cr}.

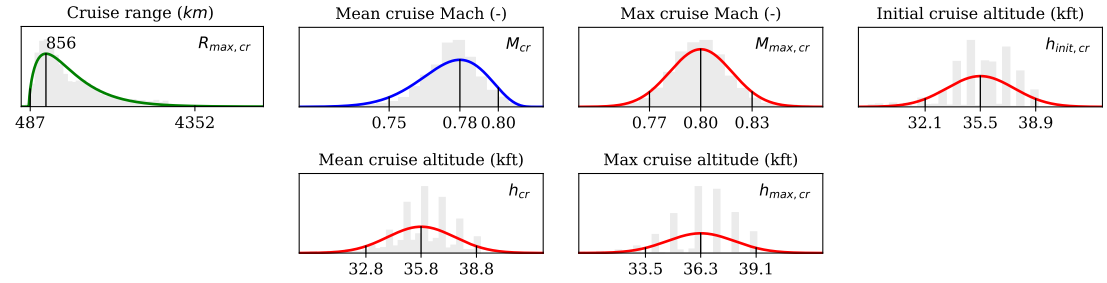

Figure 12: Cruise parameters

Unlike other performance parameters, the cruise range R_{cr} is spread very widely, where 99% of flights globally range from 487 km to 4352 km. This reflects the broad usage of the A320. However, most common flights for this type cruise with a range of less than 1000 km operationally.

5.1.5. Descent

Similar to climb, the descent phase can also be modeled as a constant Mach descent segment and a constant CAS descent segment. The parameters are shown in Fig. 13. Most commonly, the aircraft starts its initial descent at a constant Mach number of 0.77 and a vertical rate of -1128 ft/min, until reaching an altitude of 31.6 kft. It then starts a constant CAS descent of 281 kt and vertical rate of -1974 ft/min until reaching the altitude 18.9 kft. Then, the aircraft descends with a vertical rate of -1196 ft/min until final approach. The last plot shows the range from top-of-descent to destination, typically around 234km.

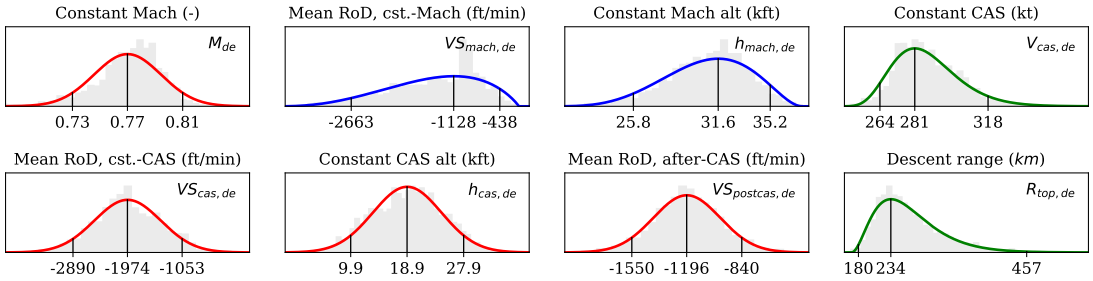

Figure 13: Descent parameters

It is worth taking into consideration that the results obtained from the dataset contain both CDA and non-CDA descent approaches.

5.1.6. Final Approach

At final approach, airspeed $V_{cas,fa}$ and vertical rate VS_{fa} are shown in Fig. 14, which are 140 kt and -698 ft/min respectively. The last two plots show the variance of these two parameters within each trajectory. Similar to the initial climb, the quasi-constant airspeed and vertical rate assumption are still valid. The path angle obtained during the final approach is around 3 degrees.

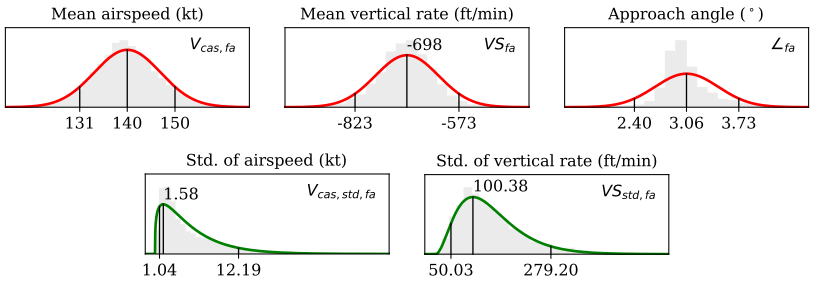

Figure 14: Final approach parameters

5.1.7. Landing

For the landing phase, approach speed V_{tcd}, braking distance d_{lnd}, and mean deceleration $\bar{a}_{lnd}$ are shown in Fig. 15, with values of around 134 kt, 1.08 km, and -1.22 $\mathrm{m/s^2}$. Braking distance shows a large variance, ranging from around 600 meters to more than 3km. Different factors such as aircraft weight, wind direction, and runway conditions would all cause such large deviations.

5.2. Correlations

There is usually an interdependence between parameters within each phase. For instance, with higher acceleration, the takeoff distance would be reduced. In order to reveal these relationships,

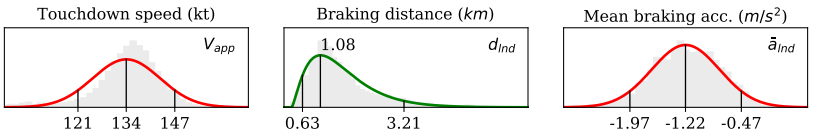

Figure 15: Landing parameters

a correlation matrix is computed for each combination of parameters and illustrated using a correlation plot.

In the following graphs, correlations are computed and visualized. The Pearson correlation coefficient (denoted as r) of two variables x and y is computed as:

$$r = \frac{\sum_i (x_i - \bar{x})(y_i - \bar{y})}{\sqrt{\sum_i (x_i - \bar{x})^2}\sqrt{\sum_i (y_i - \bar{y})^2}} \tag{22}$$

where $\bar{x}$ and $\bar{y}$ are the means of two vectors. When r is close to 1, the variables are positively correlated. When r is close to -1, variables are negatively correlated. When r is close to 0, there is no correlation between the two variables. In all the following correlation plots, blue colors show positive correlations, while red colors indicate negative correlations. Other than displaying computed Pearson correlation coefficient values, ellipses are also used to show the degree of correlation.

In Figure 16, acceleration is highly correlated with the distance and velocity parameters. This is to be expected as they are always closely related during takeoff.

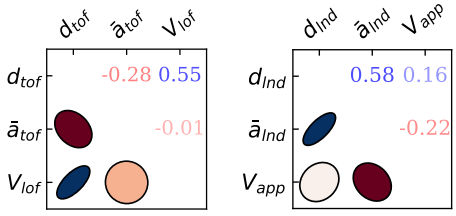

Figure 16: Takeoff and landing parameter correlations (blue = positive , red = negative)

While in Figure 17, during the cruise, for instance, it is possible to see a negative correlation between cruise altitude and cruise range.

From Figure 18, it possible to conclude that during the initial climb, the two parameters that are of interest (horizontal and vertical speed) are not significantly correlated. During the final approach, however, they show a strong negative correlation, which indicates a shallow angle for higher speed approaches.

During the climb phase, as shown in Figure 19, strong positive correlations appear between constant CAS and Mach crossover altitudes, vertical speeds, and velocities and range. Strong negative correlations appear among vertical speeds, range, and velocities, which firmly indicates the law of energy rates during the climbing performance.

In Figure 19, regarding the descent performance parameters, we can also see similar correlations as described earlier in the climb phase, with the exception that the crossover altitude of constant CAS descent to deceasing CAS demonstrates low correlations with all other parameters. This is possibly due to variation in approach procedures among airports around the world.

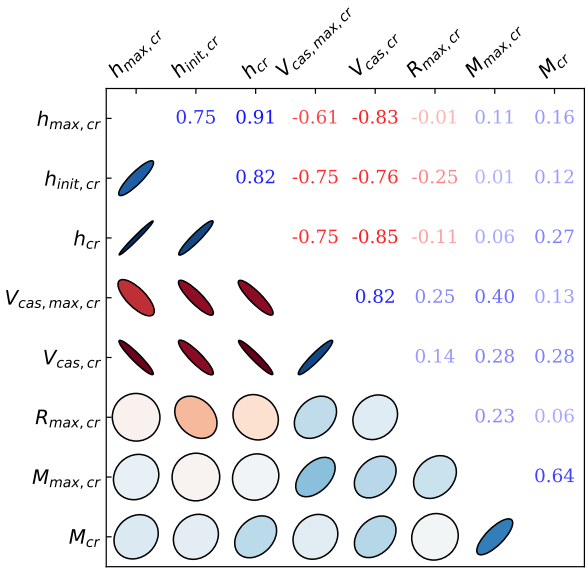

Figure 17: Cruise parameter correlations (blue = positive , red = negative)

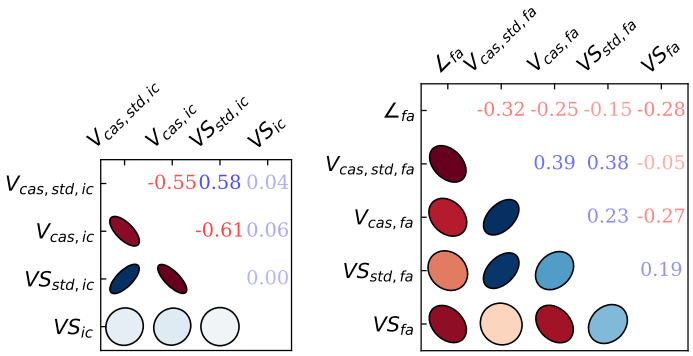

Figure 18: Initial climb and final approach parameter correlations (blue = positive , red = negative)

5.3. Comparsion for common aircraft types

The same methods and analysis are applied on a much larger dataset that contains multiple aircraft types. Due to the complexity of displaying all distribution and models for all parameters and aircraft types, the optimal parameter values of 17 aircraft types are shown in Table 2. To harmonize the unit, we follow the International System of units instead of aeronautical units in this summary table. Corresponding aircraft types of the ICAO designators can be found in reference (ICAO, 2018).

6. Validations

The performance parameters in the WRAP model are all derived from large numbers of flight data, which resemble the best estimates of how aircraft truly perform. There are a few existing performance models that can be used as references to examine the validity of the estimated parameters. BADA (version 3.12) (Nuic, 2014) and Eurocontrol Aircraft Performance Database (EuroControl, 2017) are used for comparison. However, not all parameters present in the WRAP

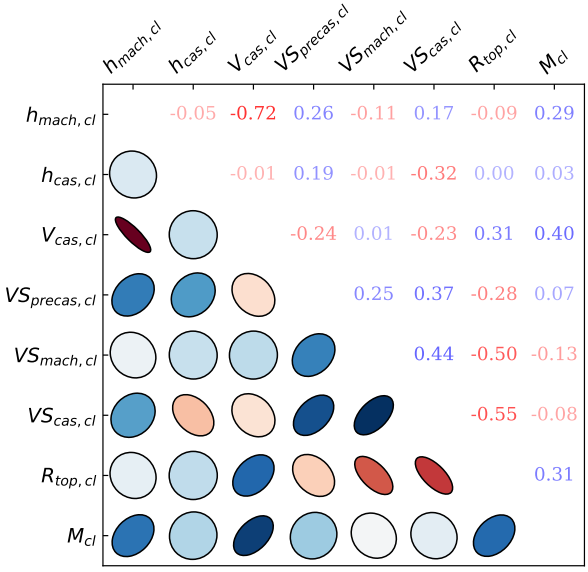

Figure 19: Climb parameter correlations (blue = positive , red = negative)

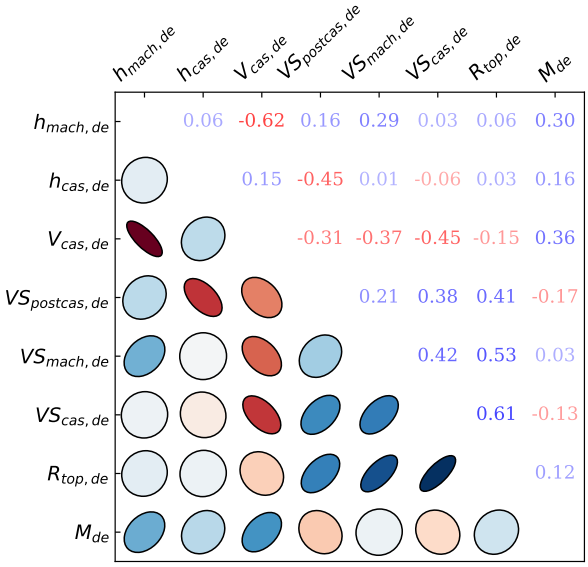

Figure 20: Descent parameter correlations (blue = positive , red = negative)

model are available in these two existing models. Therefore, only the commons parameters are compared.

Within the BADA (version 3.12), similar performance parameters are contained in the OPF (Operational Performance File) and APF (Airline Procedure File). The differences between BADA and WRAP on ten performance parameters (from 14 aircraft types) are shown in Fig. 21.

It can be observed that most parameters from different aircraft types are very close to what is presented in BADA, with the exception that takeoff distance (d_{tof}) is around 20% lower than for BADA. This is likely due to the maximum takeoff weight assumed in the BADA model. The same applies to the landing distance. In BADA, the landing distance is also based on the maximum landing weight, under dry, hard, level runway under ISA conditions with no wind.

Table 2: Optimal performance parameters for various commercial aircraft

Phase	Param	Unit	A319	A320	A321	A332	A333	A343	A388	B737	B738	B739	B744	B752	B763	B77W	B788	B789	E190
TO	V_{lof}	m/s	82.7	85.3	90.8	89.9	89.9	87.0	89.9	83.6	86.5	91.3	92.4	90.5	92.4	96.4	90.3	96.1	88.1
	d_{tof}	km	1.51	1.65	1.85	1.97	1.86	2.16	2.56	1.50	1.64	1.91	2.29	1.70	1.82	2.21	2.16	2.49	1.80
	$\bar{a}_{tof}$	m/s^2	1.84	1.93	1.95	1.75	1.72	1.40	1.35	1.77	1.82	1.87	1.67	1.91	1.97	1.89	1.61	1.63	1.83
IC	VS_{ic}	m/s	80	83	86	86	87	84	88	81	87	91	91	88	88	98	87	92	78
	$V_{cas,ic}$	m/s	12.27	12.59	13.21	12.48	12.28	6.44	5.65	11.93	12.27	12.36	9.24	12.99	14.28	13.02	10.65	10.60	11.19
CL	$R_{top,cl}$	km	206	257	230	297	287	293	296	204	216	239	223	220	202	214	286	263	215
	$V_{cas,cl}$	m/s	149	151	155	152	153	155	163	151	151	154	168	155	159	164	158	163	140
	M_{cl}	-	0.77	0.78	0.77	0.81	0.80	0.78	0.84	0.78	0.77	0.78	0.84	0.79	0.79	0.83	0.85	0.84	0.75
	$h_{cas,cl}$	km	3.2	3.7	3.7	3.6	3.1	3.6	3.3	3.4	3.6	3.4	3.9	4.0	4.0	3.8	3.8	4.1	3.0
	$h_{mach,cl}$	km	8.9	8.8	8.4	9.2	9.1	8.5	8.9	8.9	8.9	8.6	8.3	8.7	8.3	8.8	9.5	9.1	9.2
	$VS_{precas,cl}$	m/s	11.10	10.25	9.38	9.53	8.82	6.54	7.85	11.40	10.61	10.18	8.66	10.29	10.16	8.99	9.58	9.46	10.44
	$VS_{cas,cl}$	m/s	10.15	8.43	8.17	7.98	7.65	6.59	7.51	11.71	10.24	8.88	8.77	8.95	10.26	8.55	9.02	8.68	8.93
	$VS_{mach,cl}$	m/s	6.07	5.28	5.19	5.23	4.56	4.08	5.56	6.74	6.20	5.55	6.72	6.23	6.95	5.76	6.02	6.05	4.82
CR	$R_{max,cr}$	km	4019	4352	5338	11012	8911	13929	20565	4929	4953	4458	12725	6087	9544	14177	11619	14555	2710
	$V_{cas,cr}$	m/s	125	133	138	129	131	138	136	122	130	138	146	131	137	148	132	139	131
	$V_{cas,max,cr}$	m/s	128	135	140	135	137	149	145	126	132	145	157	138	142	159	139	148	137
	M_{cr}	-	0.77	0.78	0.78	0.81	0.81	0.81	0.84	0.78	0.78	0.78	0.84	0.79	0.80	0.84	0.85	0.85	0.77
	$M_{max,cr}$	-	0.80	0.80	0.80	0.84	0.83	0.83	0.86	0.80	0.80	0.81	0.87	0.82	0.83	0.86	0.87	0.87	0.81
	$h_{init,cr}$	km	11.54	10.82	10.34	11.33	11.10	10.01	11.55	12.52	11.13	10.43	10.28	11.00	10.65	9.63	11.65	11.30	10.99
	h_{cr}	km	11.54	10.92	10.41	11.67	11.49	10.86	11.73	11.74	11.23	10.52	10.81	11.17	10.81	10.35	12.01	11.58	11.05
	$h_{max,cr}$	km	11.64	11.06	10.56	11.95	12.53	11.70	12.06	11.90	11.38	10.74	11.29	11.64	11.17	11.00	12.28	11.99	11.16
DE	$R_{top,de}$	km	233	234	236	283	284	281	310	244	241	245	262	247	244	257	292	293	253
	M_{de}	-	0.76	0.77	0.77	0.81	0.81	0.81	0.83	0.78	0.77	0.78	0.83	0.79	0.79	0.82	0.84	0.84	0.77
	$V_{cas,de}$	m/s	145	144	150	152	150	154	154	146	145	148	152	151	151	156	153	154	148
	$h_{mach,de}$	km	9.2	9.6	9.0	10.2	10.2	9.9	10.1	9.6	9.7	9.4	10.0	9.4	9.5	9.7	10.5	10.5	9.3
	$h_{cas,de}$	km	5.3	5.7	6.2	6.3	6.3	5.8	6.6	5.7	5.9	6.5	6.6	6.3	6.7	6.7	7.0	7.0	5.4
	$VS_{mach,de}$	m/s	-5.87	-5.76	-5.52	-6.28	-6.17	-5.84	-6.06	-5.63	-5.80	-4.78	-5.43	-6.80	-6.29	-7.04	-7.59	-7.16	-5.25
	$VS_{cas,de}$	m/s	-9.84	-10.03	-9.41	-9.39	-9.03	-9.27	-8.36	-9.39	-9.95	-8.96	-9.17	-9.56	-9.98	-9.05	-9.52	-9.14	-9.08
	$VS_{postcas,de}$	m/s	-5.88	-6.08	-6.01	-5.82	-5.74	-5.50	-5.48	-5.85	-6.23	-6.02	-6.29	-6.16	-6.29	-6.30	-6.20	-6.19	-5.90
FA	$V_{cas,fa}$	m/s	67	72	75	72	73	74	73	70	77	78	79	69	74	78	75	77	70
	VS_{fa}	m/s	-3.42	-3.55	-3.69	-3.62	-3.74	-3.64	-3.71	-3.58	-3.84	-3.92	-4.03	-3.41	-3.76	-4.03	-3.99	-4.15	-3.57
	$\angle_{fa}$	°	3.15	3.06	3.01	2.98	2.97	3.04	2.90	3.08	3.02	3.03	2.98	3.09	2.98	2.95	2.88	2.89	2.92
LD	V_{app}	m/s	66.2	69.4	72.9	70.7	71.5	72.2	70.0	68.8	75.4	76.8	77.9	66.7	72.1	76.9	71.3	74.0	66.9
	d_{lnd}	km	1.38	1.08	1.55	1.54	1.48	1.65	2.26	1.91	1.25	1.45	1.64	1.21	1.51	1.49	2.08	2.49	2.10
	$\bar{a}_{lnd}$	m/s^2	-0.87	-1.22	-1.21	-1.18	-1.20	-1.01	-1.01	-0.83	-1.36	-1.33	-1.18	-1.03	-1.10	-1.33	-1.12	-1.11	-1.08

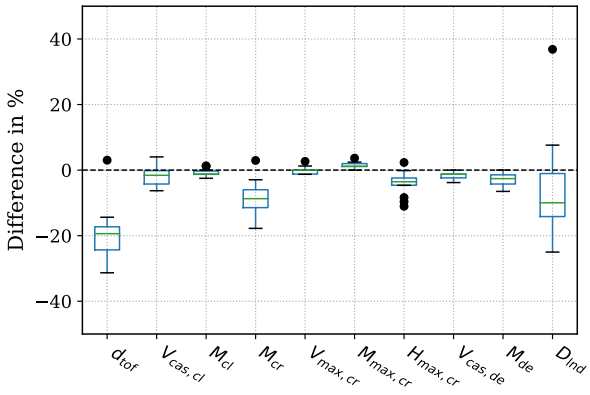

Figure 21: Comparison with BADA

In a similar fashion, the Eurocontrol Aircraft Performance Database can also be used as a source for comparison. It provides more performance parameters, which are used primarily for training purposes on a wide range of commercial and military aircraft. A total of 17 parameters from 14

aircraft that exist in both models are compared. The result is shown in Fig. 22.

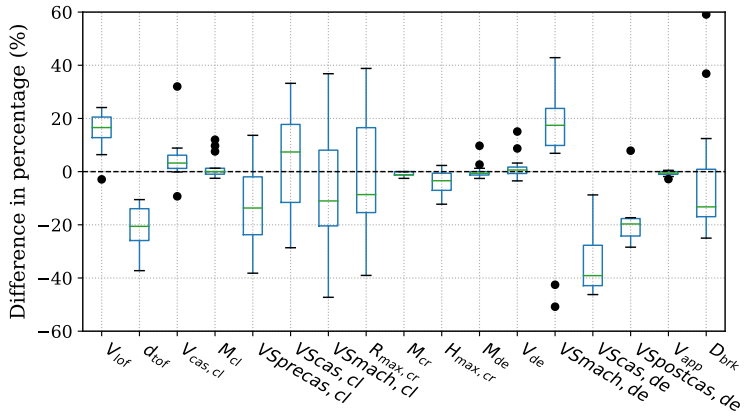

Figure 22: Comparison with Eurocontrol Aircraft Performance Database

The parameters that show large bias are the different vertical rates during the descent phase. In the Eurocontrol database, it is common that the second descent segment has a much higher vertical rate. However, this trend is not significant in the flight data as observed. It can also be the case that the crossover altitudes obtained from data in WRAP model are different from the fixed crossover altitude from the Eurocontrol database.

Furthermore, compared to both BADA and the Eurocontrol database, the WRAP model also includes the minimum value, maximum value, and a parametric model for each parameter.

7. Discussions

7.1. Geo-correlation of performance parameters

The flights used for this paper are distributed all over the world, which means the obtained distributions of parameters reflect combinations of the performance of all airspaces that are present in the dataset. The advantage of such a dataset is that it gives a complete view of performance from different areas globally. On the other hand, some of these distributions may not be able to reflect certain airspaces, countries or airports accurately due to controller procedures or airport limitations, etc. These geographically different situations may especially affect data from departure and arrival segments of flights. The correlation between performance indicators and locations are not studied in this paper. Hence, no conclusion can be drawn whether the distributions would be significantly different between different locations. This could, however, be an interesting topic for future research.

7.2. Point of lift-off and touch-down

During the takeoff and landing phases, because of the low data update rate, the estimation method illustrated in Fig. 4 is used to locate the most likely lift-off or touch-down moment, from which related parameters are interpolated.

Statistically, there are relatively large gaps between the last on-ground data point and the first in-air data point. Fig. 23 shows the time gaps (Δt) observed in the dataset from this study (takeoffs and landings of around 7000 flights).

Most commonly, the Δt is about three to nine seconds during which the aircraft would have flown, climbed, or descended for a fairly large distance. Thus, when dealing with such data, using

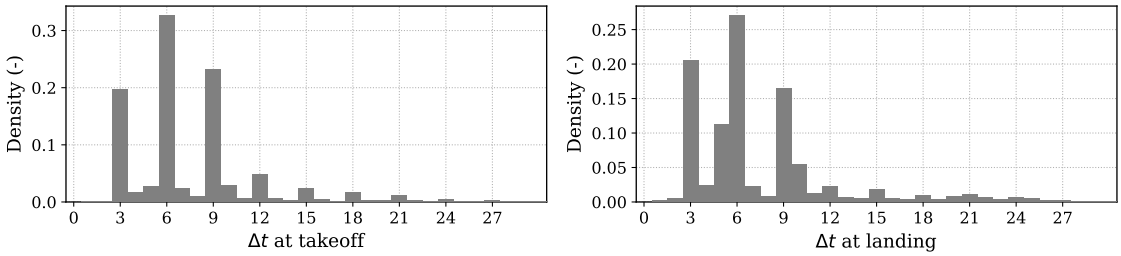

Figure 23: Time gap between two data points at takeoff and landing

the above method improves the accuracy of parameter estimations during the phases where fewer samples are available. However, the extrapolated liftoff time and speed would diverge from actual values.

It is also interesting to note that there is a three-second time gap in both figures for takeoff and landing. This is likely due to the update rate of aggregated ADS-B data used in this paper. When considering raw ADS-B data, this gap can be reduced to a half second if receivers are in a good line-of-sight range of the taking off or landing aircraft.

7.3. Speed restrictions

It is not uncommon that speed restrictions are imposed by air traffic control for aircraft below a certain altitude. In many airspaces, this restriction is set to be 250 kt below 10,000 ft. In the WRAP model, such a restriction is left out due to the fact that it is hard to generalize this rule for all aircraft models and different airspaces. In Figure 24, the calibrated airspeed of Airbus aircraft are shown. We can see that for a majority of the flight, such speed restrictions exist, especially for smaller aircraft types. However, for heavier aircraft types like A380 or A340, the speed restriction cannot always be maintained.

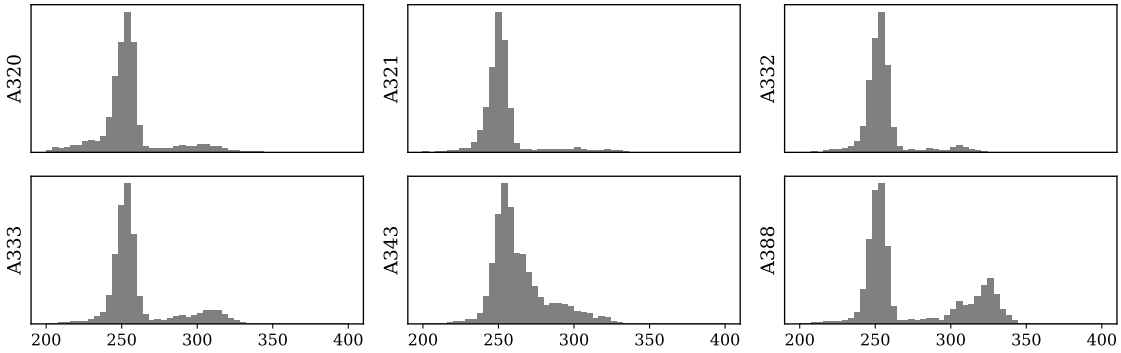

Figure 24: Calibrated airspeed at 10000 feet per aircraft type

This procedure limitation does influence parameter modeling. In this paper, we used a piecewise model (as shown in Equation 16) to extract the climb profiles. The quadratic function allows us to handle data under different operating procedures.

Even though the WRAP model does not define this speed restrictions, it is not hard for future users to implement similar control logic into their own scenarios. Then from 10,000 ft above, the WRAP model parameter can be used.

7.4. Cruise altitude

It is apparent from Figure 12, that the cruise altitude cannot be well described by a continuous distribution. A discrete distribution would be better placed to capture the selection of discrete cruise flight levels. However, for the uniformity of the model parameters, the continuous density is assumed. Nevertheless, the mean and maximum values found from the Normal distribution can still be used in most user scenarios.

Another common procedure that is not described in this paper is the step climbs for long-haul flights. With the decreasing aircraft mass due to fuel consumption, the optimal cruise altitude increases. Airliners often perform step climbs to avoid the continuous change of aircraft altitude, though it is less efficient as pointed by Dalmau and Prats (2015). It is difficult to model the step climb when compared to other parameters in the WRAP model. First of all, step climbing is a discrete process and happens only for long-haul flights. For long-haul flights, there are often large missing segments in the cruise phase due to limitations in ADS-B receiver coverage. As a result, important climbing data may be omitted/missing. Secondly, to accurately model the step climb, we must know the mass and fuel flow model of the aircraft. The estimation of these parameters is possible but complicated. In our earlier research (Sun et al., 2018), we have demonstrated the estimation of mass and fuel flow based on ADS-B data. However, the estimation has to rely on the BADA kinetic model, which contradicts the intention of WRAP as an open model.

Given these complexities, we have left step climbs out of this paper. However, by using the existing parameters $h_{init,cr}$, h_{cr}, and $h_{max,cr}$, one can construct a continuous cruise climbing profile from initial cruise altitude to the top of descent.

7.5. Continuous descents

To maximize the fuel efficiency and when it is allowed by air traffic controllers, aircraft often perform continuous descent approaches (CDA) in order to save fuel and reduce noise. However, when modeling the aircraft performance, CDA has an impact on some parameters during the entire descent phase. To study the influence of this factor, a similar number of CDA and non-CDA flights (around 3000 flights each) are used. All parameters related with descent are computed and compared in parallel. There are different ways of defining CDA. In this paper, we considered CDA for flights that do not contain any level-off during the descent.

As shown in Fig. 25, eight parameters in CDA and non-CDA flights are shown. Crossover altitudes and velocities of constant Mach/CAS descent do not change between these two approaches, but other parameters show large differences. In the first sub-figure, it is clear that performing a CDA decreases the range of top-of-descent drastically. From sub-figure six to eight, it is also apparent that the descent rates are all increased under CDA. All of these differences are indeed aligned with the definition of CDA. However, other than the range of descent, by separating the cases of CDA and non-CDA, the accuracy for other parameter models do not show significant increases. As a result, the generic models are still proposed for the descents phase. Nevertheless, as an additional precaution, such operational influences should not be neglected when it comes to flight data mining and analytics.

7.6. Data and model use cases

ADS-B data are not distributed equally per aircraft type. The same amount of data from most common aircraft types such as Airbus-320 and Boeing-737 can be collected within a week, while for other less common aircraft types such as Airbus-380 and Boeing-777, this process may take several months. While completing this research, a total of 1.6 million flights have been captured

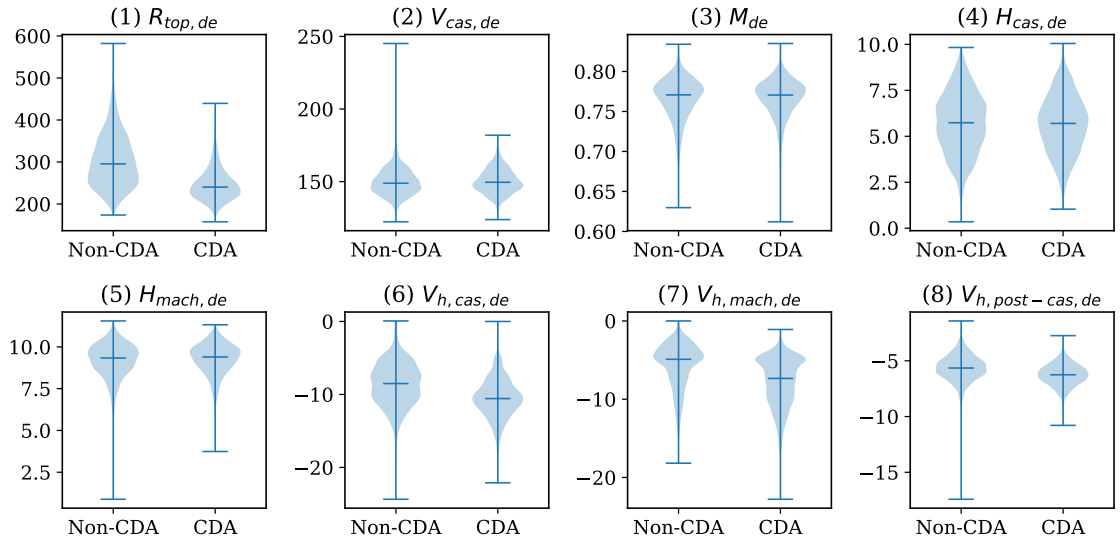

Figure 25: Comparing descent parameters during CDA and Non-CDA

during a period of five months for around 30 commercial aircraft types. However, with the constant flow of new ADS-B data, the models can be continuously improved and extended.

The current WRAP model and future updates are published under the GNU open source license. Parameters from the model have been adopted in the BlueSky Open Air Traffic Simulator (Hoekstra and Ellerbroek, 2016) as one of the core performance models of flight envelopes. At a broader scale, both methods and models addressed in this paper can be beneficial for other use cases, for example, probability density function based Monte-Carlo simulations and aircraft performance comparison studies.

8. Conclusions

In this paper, we primarily discuss the process of utilizing Automatic Dependent Surveillance-Broadcast (ADS-B) data collected by large crowd-sourced networks to construct aircraft kinematic performance models. The entire process consists of flight data processing, aggregating atmospheric data using external sources, developing methods that extract performance parameters, and designing parametric statistical models, as well as examining the final WRAP model. As a result, a total of 32 parameters per aircraft type are presented in the current version of the WRAP model, covering the 17 most common aircraft types. The models for the 17 aircraft types are summarized in this paper and shared under an open-source license. Comparison studies are performed against existing models such as Eurocontrol Base of Aircraft Data (BADA) and Eurocontrol Aircraft Performance Database.

The WRAP aircraft performance model is constructed based on global flight data observed over an extended period of time. It is not designed to reflect different local variations in the air traffic management sectors. Short-term variations are also not considered in this paper, which poses a limitation for the resulting model. However, the set of methods proposed in the paper does allow us to produce similar models using user-defined spatial and temporal filtering. This potential is enabled by the re-usability of modeling methods proposed in this paper, which are essential for dealing with ADS-B flight data. The combined framework gives other researchers the possibility to reproduce the results and apply our methods for similar studies.

When compared to BADA, the WRAP model cannot replace BADA's kinetic performance model (OPF). Like other kinematic models, WRAP is not designed for the purpose of single trajectory prediction or optimization. This is the main limitation of the WRAP model. However, it is a good alternative to the BADA procedural performance model (APF) or GAME performance model. It aims to serve as a realistic model for applications where only kinematic performance models are needed. The creation of an additional open kinetic performance model that is comparable to BADA OPF remains a topic of great interest in our separate research projects.

It is worth emphasizing that the WRAP model not only defines procedural parameters but also proposes parametric statistical models for these parameters. These statistical models can be used conveniently to conduct Monte-Carlo simulations. The maximum and minimum parameter values in WRAP can be used as performance limitations in simulations. This property enables extended capabilities for aircraft performance based studies, such as large-scale 4D trajectory simulations and air traffic optimizations. As compared to existing performance models, the openness of the model will increase the reproducibility of future studies. At the same time, with the increase in data gathered by ADS-B receiver networks, the accuracy and aircraft type varieties of the model will be gradually improved.

9. Acknowledgment

We would like to thank FlightRadar24 and its network of contributors for the open data that helped to construct this research paper. We would also like to thank Julia Rudnyk for the feedback that improved the KS test in this paper. The WRAP model is shared on GitHub platform at https://github.com/junzis/wrap.

References

Aldrich, J., et al., 1997. RA Fisher and the making of maximum likelihood 1912-1922. Statistical Science 12 (3), 162–176.

Calders, P., 2002. G.A.M.E. Aircraft Performance Model Description. Eurocontrol, DIS/ATD Unit, DOC.CoE-TP-02002.

Choi, S., Wette, R., 1969. Maximum likelihood estimation of the parameters of the gamma distribution and their bias. Technometrics 11 (4), 683–690.

Commercial Aviation Safety Team / Common Taxonomy Team, 2013. Phase of Flight: Definitions and Usage Notes 1.3 (April), 1–11.

Dalmau, R., Prats, X., 2015. Fuel and time savings by flying continuous cruise climbs: Estimating the benefit pools for maximum range operations. Transportation Research Part D: Transport and Environment 35, 62–71.

EuroControl, 2017. EuroControl Aircraft Performance Database. `https://contentzone.eurocontrol.int/aircraftperformance`, accessed on August 2017.

FlightRadar24 AB, 2017. FlightRadar24, Terms and Conditions, Item 9. `http://www.flightradar24.com/terms-and-conditions`, accessed on August 2017.

Gallo, E., Navarro, F. A., Nuic, A., Iagaru, M., 2006. Advanced aircraft performance modeling for ATM: BADA 4.0 results. In: 25th Digital Avionics Systems Conference, 2006 IEEE/AIAA. IEEE, pp. 1–12.

Gnanadesikan, R., Pinkham, R., Hughes, L. P., 1967. Maximum likelihood estimation of the parameters of the beta distribution from smallest order statistics. Technometrics 9 (4), 607–620.

Hempe, D. W., 2010. Airworthiness Approval of Automatic Dependent Surveillance-Broadcast (ADSB) Out Systems. Advisory Circular 20-165.

Hoekstra, J., Ellerbroek, J., 2016. BlueSky ATC Simulator Project: an open Data and Open Source Approach. In: Proceedings of the 7th International Conference on Research in Air Transportation.

Hrastovec, M., Solina, F., 2016. Prediction of aircraft performances based on data collected by air traffic control centers. Transportation Research Part C: Emerging Technologies 73, 167–182.

ICAO, 2018. DOC 8643 - Aircraft Type Designators. International Civil Aviation Organization. URL https://www.icao.int/publications/DOC8643

Massey Jr, F. J., 1951. The Kolmogorov-Smirnov test for goodness of fit. Journal of the American statistical Association 46 (253), 68–78.

Mohleji, S. C., Wang, G., 2010. Modeling ADS-B position and velocity errors for airborne merging and spacing in interval management application. MITRE release, 10–3026.

Nuic, A., 2009. Base of Aircraft Data (BADA) Product Management Document. Tech. rep., Tech. Rep. EEC Technical/Scientific Report.

Nuic, A., 2014. User manual for the Base of Aircraft Data (BADA) revision 3.12. Atmosphere 2014.

Saha, S., Moorthi, S., Pan, H.-L., Wu, X., Wang, J., Nadiga, S., Tripp, P., Kistler, R., Woollen, J., Behringer, D., et al., 2010. The NCEP climate forecast system reanalysis. Bulletin of the American Meteorological Society 91 (8), 1015–1057.

Schäfer, M., Strohmeier, M., Lenders, V., Martinovic, I., Wilhelm, M., 2014. Bringing up OpenSky: A large-scale ADS-B sensor network for research. In: Proceedings of the 13th international symposium on Information processing in sensor networks. IEEE Press, pp. 83–94.

Sun, J., Ellerbroek, J., Hoekstra, J., 2017a. Flight Extraction and Phase Identification for Large Automatic Dependent Surveillance–Broadcast Datasets. Journal of Aerospace Information Systems 14 (10), 566–571.

Sun, J., Ellerbroek, J., Hoekstra, J., 2017b. Modeling aircraft performance parameters with open ADS-B data. In: Proceedings of the 12th USA/Europe Air Traffic Management Research and Development Seminar. FAA/EUROCONTROL.

Sun, J., Ellerbroek, J., Hoekstra, J. M., 2018. Aircraft initial mass estimation using Bayesian inference method. Transportation Research Part C: Emerging Technologies 90, 59–73.

Weiser, A., Zarantonello, S. E., 1988. A note on piecewise linear and multilinear table interpolation in many dimensions. Mathematics of Computation 50 (181), 189–196.

Young, T. M., 2017. Performance of the Jet Transport Airplane: Analysis Methods, Flight Operations, and Regulations. John Wiley & Sons.